British Journal of Pharmacology

British Journal of Pharmacology (2018) **175** 1731–1743 1731

RESEARCH PAPER

Novel long-acting antagonists of muscarinic ACh receptors

Correspondence Jan Jakubík, Department of Neurochemistry, Institute of Physiology CAS, Videnska 1083, CZ 142 20, Prague, Czech Republic. E-mail: jan.jakubik@fgu.cas.cz

Received 11 October 2017; **Revised** 24 January 2018; **Accepted** 15 February 2018

Alena Randáková[1], Vladimír Rudajev[1], Vladimír Doležal[1], John Boulos[2] and Jan Jakubík[1]

[1]Department of Neurochemistry, Institute of Physiology, Czech Academy of Sciences, Prague, Czech Republic, and [2]Department of Physical Sciences, Barry University, Miami Shores, FL, USA

BACKGROUND AND PURPOSE

The aim of this study was to develop potent and long-acting antagonists of muscarinic ACh receptors. The 4-hexyloxy and 4-butyloxy derivatives of 1-[2-(4-oxidobenzoyloxy)ethyl]-1,2,3,6-tetrahydropyridin-1-ium were synthesized and tested for biological activity. Antagonists with long-residence time at receptors are therapeutic targets for the treatment of several neurological and psychiatric human diseases. Their long-acting effects allow for reduced daily doses and adverse effects.

EXPERIMENTAL APPROACH

The binding and antagonism of functional responses to the agonist carbachol mediated by 4-hexyloxy compounds were investigated in CHO cells expressing individual subtypes of muscarinic receptors and compared with 4-butyloxy analogues.

KEY RESULTS

The 4-hexyloxy derivatives were found to bind muscarinic receptors with micromolar affinity and antagonized the functional response to carbachol with a potency ranging from 30 nM at M_1 to 4 μM at M_3 receptors. Under washing conditions to reverse antagonism, the half-life of their antagonistic action ranged from 1.7 h at M_2 to 5 h at M_5 receptors.

CONCLUSIONS AND IMPLICATIONS

The 4-hexyloxy derivatives were found to be potent long-acting M_1-preferring antagonists. In view of current literature, M_1-selective antagonists may have therapeutic potential for striatal cholinergic dystonia, delaying epileptic seizure after organophosphate intoxication or relieving depression. These compounds may also serve as a tool for research into cognitive deficits.

Abbreviations

KHB, Krebs-HEPES buffer; NMS, *N*-methylscopolamine; TCA, trichloracetic acid

DOI:10.1111/bph.14187

Introduction

Muscarinic ACh receptors are located in the plasma membrane of many cell types of various tissues and mediate extracellular to intracellular signalling. They are involved in the control of numerous central and peripheral physiological responses, as well as being an important drug target in human disease (Eglen, 2012). This family of receptors comprises muscarinic receptors denoted as M_1–M_5 (Bonner, 1989). Selective muscarinic antagonists have great therapeutic potential. Muscarinic **M_2** and **M_3 receptors** mediate contraction of smooth muscles (Ehlert, 2003) are thus possible therapeutic targets for the treatment of airway disorders including asthma/chronic obstructive pulmonary disease and overreactive bladder syndrome. Cholinergic neurons are key modulators of basal ganglia function the impairment of which is involved in Parkinson's disease (PD) (Lester *et al.*, 2010). The M_1 selective muscarinic antagonist **VU0255035** has been identified as a possible treatment of PD (Xiang *et al.*, 2012). Cholinergic interneurons modulate dopamine-dependent activities, including locomotion, *via* **M_4 receptors** expressed on dopamine neurons (Jeon *et al.*, 2010). This also indicates the possible use of M_4 selective antagonists in PD treatment. **M_5 receptors**, almost exclusively expressed in the CNS, primarily the substantia nigra and ventral tegmental brain areas, play a major role in the rewarding effects of compound abuse (Eglen, 2012). Knockout of the M_5 receptor led to a reduction in cocaine self-administration in mice (Thomsen *et al.*, 2005), suggesting that M_5 antagonists may be an important approach for developing novel therapeutics for drug addiction.

Antagonists with long-residence time at receptors are longer acting, thus allowing for lower daily drug doses to reach a maximum therapeutic effect. Currently, only several long-acting muscarinic ligands have been discovered (Disse *et al.*, 1993; Christopoulos *et al.*, 1998; Prat *et al.*, 2009; Ulrik, 2012; Heusler *et al.*, 2015). A structure–activity relationship study revealed that the long action of the N-substituted tetrahydropyridine based agonist **xanomeline** is conditioned by the hexyloxy chain in its structure (Jakubík *et al.*, 2004). In view of this finding, novel N-substituted tetrahydropyridine comprising antagonists, namely, 4-hexyloxy derivatives of 1-[2-(4-oxidobenzoyloxy)ethyl]-1,2,3,6-tetrahydropyridin-1-ium were synthesized and tested for biological activity. Several of these compounds were found to be long-acting antagonists and, similar to the agonist xanomeline, act preferentially at the M_1 receptor subtype. These compounds may have therapeutic potential for striatal cholinergic dystonia (Eskow Jaunarajs *et al.*, 2015), delaying epileptic seizures after organophosphate intoxication (Miller *et al.*, 2017) or relieving depression (Navarria *et al.*, 2015). They may also serve as a tool in research into cognitive deficits (Klinkenberg and Blokland, 2010).

Methods

Synthesis

Reagents for synthesis were purchased from Aldrich Chemical Company (St. Louis, MO), and all starting liquid materials were distilled before use. NMR spectra were recorded on a Varian 300 MHz spectrometer. GC–MS spectra were recorded on a Perkin Elmer Clarus 500 and 560S system. Elemental analyses were carried out by Galbraith Laboratories (Knoxville, TN). Melting points were recorded on a Digimelt MPA160 purchased from Stanford Research Systems. Refractive indexes were recorded on r^2 i300 digital refractometer from Reichert Technologies corrected for 20°C. Compounds **1** and **2** (Figure 1) were synthesized by reaction of pyridine with 2-bromoethanol. The product was selectively reduced with sodium borohydride to yield 2-(3,4-dihydro-2H-pyridin-1-yl)ethanol. This alcohol was then coupled with para-substituted benzoyl chlorides (R_1 = O-butyl or O-hexyl) to yield compounds **1** and **2,** which were then treated with hydrogen chloride gas and iodomethane to yield salts **11**, **12** and **21**, **22** respectively. For details, see Boulos *et al.* (2018).

Materials

Newly synthesized compounds were dissolved in buffer up to 50 mM concentration. All radiolabelled compounds [**N-[^{3}H]-methyl scopolamine** (NMS), myo-[2-^{3}H(N)]-inositol and [2,8-^{3}H]-**adenine**] were purchased from American Radiolabeled Chemicals, Inc. (Saint Louis, MO). Common

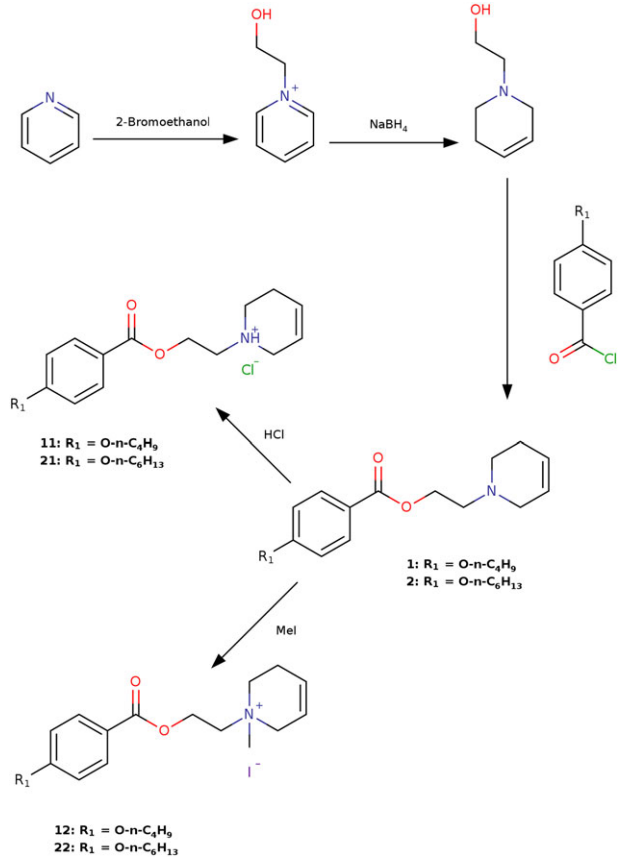

Figure 1

Reaction scheme of synthesis. Reaction scheme of synthesis of 1-[2-(4-oxidobenzoyloxy)ethyl]-1,2,3,6-tetrahydropyridin-1-ium derivatives.

chemicals were purchased from Sigma (Prague, CZ) and were of the highest purity available.

Cell culture and membrane preparation

CHO cells stably transfected with the genes of human variants of muscarinic receptors were purchased from Missouri S&T cDNA Resource Center (Rolla, MO, USA). Cell cultures and crude membranes were prepared as described previously (Boulos *et al.*, 2018). Cells were grown to confluence in 75 cm^2 flasks in DMEM supplemented with 10% FCS, and 2 million cells were sub-cultured in 100 mm Petri dishes. The medium was supplemented with 5 mM butyrate for the last 24 h of cultivation to increase receptor expression. Cells were detached by mild trypsinization on day 5 after subculture. Detached cells were washed twice in 50 mL of PBS and 3 min centrifugation at 250× *g*. Washed cells were suspended in 20 mL of ice-cold incubation medium (100 mM NaCl, 20 mM Na-HEPES, 10 mM $MgCl_2$, pH = 7.4) supplemented with 10 mM EDTA and homogenized on ice with two 30 s strokes of a Polytron homogenizer (Ultra-Turrax; Janke & Kunkel GmbH & Co. KG, IKA-Labortechnik, Staufen, Germany) with a 30 s pause between strokes. Cell homogenates were centrifuged for 30 min at 30 000× *g*. Supernatants were discarded, pellets suspended in fresh incubation medium, incubated on ice for 30 min and centrifuged again. The resulting membrane pellets were kept at −80°C until assayed within 10 weeks.

Radioligand binding

All radioligand binding experiments were optimized and carried out according to general guidelines (El-Fakahany and Jakubík, 2016). Briefly, membranes were incubated in 96-well plates at 30°C in the incubation medium described above. Incubation volume was 400 or 800 μL for competition and saturation experiments with [^{3}H]-NMS respectively. Approximately, 30 μg of membrane proteins per sample was used. NMS binding was measured directly in saturation experiments using six concentrations (30 to 1000 pM) of [^{3}H]-NMS during incubation for 1 h (M_2), 3 h (M_1, M_3 and M_4) or 5 h (M_5). For calculations of the equilibrium dissociation constant (K_D), concentrations of free [^{3}H]-NMS were calculated by subtraction of bound radioactivity from total radioactivity in the sample and fitting (Equation 1; Data analysis). Binding of tested ligands was determined in competition experiments with 1 nM [^{3}H]-NMS, and inhibition constant K_i was calculated according to Equation 3. Incubation time was 3 h (M_2), 9 h (M_1, M_3 and M_4) or 15 h (M_5). Non-specific binding was determined in the presence of 1 μM unlabelled **atropine**. Incubations were terminated by filtration through Whatman GF/C glass fibre filters (Whatman) using a Brandel cell harvester (Brandel, Gaithersburg, MD, USA). In kinetic experiments, membranes were pre-incubated with 1 nM [^{3}H]-NMS for 1 h (M_2), 3 h (M_1, M_3, M_4) or 5 h (M_5). Then dissociation was started by addition of atropine to the final concentration of 1 μM. Atropine was added either alone or in mixture with the compound being tested at a final concentration ranging from 10 μM to 10 mM. Dissociation was terminated by filtration. Filters were dried in a microwave oven, and then solid scintillator Meltilex A was melted on filters (105°C, 70 s) using a hot plate. The filters were cooled and counted in a Wallac Microbeta scintillation counter.

Inhibition of functional response to carbachol

Inhibitory effects of tested compounds on functional response to **carbachol** were quantified by measurement of changes in accumulation of inositol phosphates. M_2 and M_4 receptors that preferentially inhibit cAMP synthesis *via* $G_{i/o}$ G-proteins were coupled to the PLC – calcium pathway. For this purpose, new CHO cell lines stably expressing promiscuous G_{15} G-protein (Offermanns and Simon, 1995) , besides M_2 or M_4 receptor, were generated by transfection with pCMV/hygro vector and hygromycin selection. Cells were seeded in 96-well plates, 50 000 cells per well in 100 μL of DMEM. On the next day, DMEM was removed, and 50 μL of DMEM supplemented with 30 nM [^{3}H]-myo-inositol was added for 12 h. Then cells were washed with Krebs-HEPES buffer (KHB; 138 mM NaCl; 4 mM KCl; 1.3 mM $CaCl_2$; 1 mM $MgCl_2$; 1.2 mM NaH_2PO_4; 10 mM glucose; 20 mM Na-HEPES; pH = 7.4) supplemented with 10 mM LiCl. Cells were preincubated at 37°C for 30 min with the test compound at the desired concentration, and then carbachol was added for an additional 30 min. Then KHB was removed, and accumulation of inositol phosphates was stopped by addition of 50 μL of 20% trichloracetic acid (TCA). Plates were put to 4°C for 1 h; then 40 μL of TCA extract was transferred to another 96-well plate, mixed with 200 μL of Rotiszint scintillation cocktail and counted in Wallac Microbeta. Rest of TCA extract was discarded; individual wells were washed with 50 μL of 20% TCA; 50 μL of 1 M NaOH was added to each well; and plates were shaken at room temperature for 15 min. Then 40 μL of NaOH lysate was transferred to another 96-well plate, mixed with 200 μL of Rotiszint scintillation cocktail and counted in a Wallac Microbeta scintillation counter. The level of inositol phosphates was calculated as a fraction of soluble (TCA extract) to total (TCA extract plus NaOH lysate) radioactivity. When the ablity to reverse the inhibition induced by test compounds was determined, 30 min preincubation with test compounds was carried out in the absence of LiCl, then cells were washed 3 times with 100 μL KHB, incubated for either 1 or 5 h in 300 μL of fresh KHB at 37°C, again washed 3 times with 100 μL of KHB and finally incubated in the presence of 10 mM LiCl with carbachol for 30 min.

Alternatively, functional antagonism of carbachol-stimulated [^{35}S]-**GTPγS** binding to membranes, prepared from CHO cells expressing individual subtypes of muscarinic receptors, was measured. Membranes were preincubated with test compounds, carbachol and GDP at 30°C for 15 h. Then [^{35}S]-GTPγS was added, and samples were incubated for an additional 20 min (M_2 and M_4) or 30 min (M_1, M_3 and M_5). Final concentration of [^{35}S]-GTPγS was 500 pM (M_2 and M_4) or 200 pM (M_1, M_3 and M_5). Final concentration of GDP was 20 μM (M_2 and M_4) or 5 μM (M_1, M_3 and M_5). Incubation volume was 200 μL, and incubation temperature was 30°C. Incubations were terminated by filtration through Whatman GF/C glass fibre filters (Whatman) using a Brandel cell harvester (Brandel, Gaithersburg, MD, USA). Filters were dried in a microwave oven, and then solid scintillator Meltilex A was melted on filters (105°C, 70 s) using a hot plate. The filters were cooled and counted in a Wallac Microbeta scintillation counter.

Data analysis

Data from biological evaluation experiments were processed in Libre Office, analysed and then plotted using programme Grace (http://plasma-gate.weizmann.ac.il/Grace/). The data and statistical analysis comply with the recommendations on experimental design and analysis in pharmacology (Curtis *et al.*, 2015). Statistical analysis was performed using statistical package R (http://www.r-project.org). For non-linear regression analysis, the following equations were used:

[^{3}H]-NMS saturation binding.

$$y = \frac{B_{MAX} * x}{x + K_D}, \quad (1)$$

where y is specific binding at free concentration x, B_{MAX} is maximum binding capacity and K_D is equilibrium dissociation constant.

Competition binding.

$$y = 100 - \frac{100 * x}{x + \mathrm{IC}_{50}}, \quad (2)$$

where y is specific radioligand binding at concentration x of competitor expressed as per cent of binding in the absence of competitor, IC_{50} is concentration causing 50% inhibition of radioligand binding. Inhibition constant K_i was calculated as

$$K_i = \frac{\mathrm{IC}_{50}}{1 + \frac{[D]}{K_D}} \quad (3)$$

where $[D]$ is a concentration of [^{3}H]-NMS used (Cheng and Prusoff, 1973) .

Concentration response. After normalization to basal, Equation 4 was fitted to data from measurements of functional response.

$$y = 1 + \frac{(\mathrm{E}_{\mathrm{MAX}} - 1) * x^{nH}}{x^{nH} + \mathrm{EC}_{50}}, \quad (4)$$

where y is response normalized to basal (in the absence of carbachol) at ligand concentration x, $\mathrm{E}_{\mathrm{MAX}}$ is the maximal effect, EC_{50} is concentration causing half-maximal effect and n_{H} is Hill coefficient. If $n_{\mathrm{H}} < 0.8$, Equation 5 was fitted to data.

$$y = 1 + \frac{(E_{MAX1} - 1) * x}{x + \mathrm{EC}_{501}} * \frac{E_{MAX2} * x}{x + \mathrm{EC}_{502}}. \quad (5)$$

The equilibrium dissociation constant of antagonism of functional response K_{B} was calculated from the shift in EC_{50} of functional response to carbachol by antagonist according to Schild equation for a competitive antagonist, Equation 6, or an allosteric antagonist, Equation 7 (Kenakin, 2014).

$$\log(DR - 1) = \log([B]) - \log(K_B), \quad (6)$$

where DR is the ratio of EC_{50} of the functional response in the presence to the absence of antagonist B. In case Equation 5 did not fit the data, Equation 6 was used.

$$\log(DR - 1) = \log\left[\frac{[B](1 - \alpha)}{\alpha[B] + K_B}\right], \quad (7)$$

where α is a factor of cooperativity between carbachol and antagonist. In Schild analysis, both Equations 6 and 7 were fitted to data and then compared using the F-test, Equation 7 being an alternative hypothesis. $P < 0.05$ was taken to reject the null hypothesis.

Dissociation experiments. After subtraction of non-specific binding and normalization to binding in the beginning of dissociation, Equation 7 was fitted to the data.

$$y = 100 * e^{-k_{off} * x}, \quad (8)$$

where y is [^{3}H]-NMS binding at time x and k_{off} is the observed dissociation rate constant.

The apparent equilibrium dissociation constant K_{A} for binding of tested compounds to the secondary binding site based on dissociation experiments was obtained according to Lazareno and Birdsall (1995), and Equation 8 was fitted to the data:

$$y = \frac{k_0 * K_A}{X + K_A}, \quad (9)$$

where y is the observed rate of dissociation k_{off} at concentration x of tested compound and k_0 is dissociation rate induced by 1 μM atropine.

Nomenclature of targets and ligands

Key protein targets and ligands in this article are hyperlinked to corresponding entries in http://www.guidetopharmacology.org, the common portal for data from the IUPHAR/BPS Guide to PHARMACOLOGY (Harding *et al.*, 2018), and are permanently archived in the Concise Guide to PHARMACOLOGY 2017/2018 (Alexander *et al.*, 2017).

Results

Four of the recently synthesized derivatives of 1-[2-(4-oxidobenzoyloxy)ethyl]-1,2,3,6-tetrahydropyridin-1-ium (Boulos *et al.*, 2018) were thoroughly tested in radioligand and functional assays. These compounds contain both a para-substituted phenyl and tetrahydropyridinyl rings joined through an ester linkage. The oxygen atom at the para-position is either linked with a butyl or hexyl chain (Figure 1, R_1) while the nitrogen atom of the tetrahydropyridinyl ring is either hydrogenated or methylated (Figure 1, R_2). Compounds are assigned numbers **11**, **12**, **21** and **22**, in which the first number denotes either butyl (1) or hexyl (2) chain of R_1 and the second number denotes either hydrogen (1) atom or methyl (2) group of R_2 (Table 1). In competition experiments with 1 nM [^{3}H]-NMS, all four compounds completely displaced [^{3}H]NMS binding suggesting competitive interaction (Supporting Information Figure S1). Compounds **11**, **12** and **21** displayed micromolar affinity whereas K_{i} of compound **22** was submicromolar (pK_{i} varied from 6.82 ± 0.02 at M_2 to 6.36 at M_4; mean ± SD, n = 6). Binding of compounds was non-selective among receptor subtypes with exception of compounds **11** and **12** that showed slightly higher affinity at M_2 receptors (Table 1).

Table 1

Inhibition constants (K_i)

	R_1	R_2	M_1	M_2	M_3	M_4	M_5
11	Butyl	-H	5.19 ± 0.05	5.50 ± 0.05*	5.11 ± 0.05	4.95 ± 0.04	5.20 ± 0.04
12	Butyl	Methyl	5.70 ± 0.05[b]	5.71 ± 0.05[b]	5.23 ± 0.06[b]	5.11 ± 0.07[b]	5.47 ± 0.07[b]
21	Hexyl	-H	5.37 ± 0.03[ab]	5.49 ± 0.06*	5.24 ± 0.06[ab]	5.04 ± 0.05	5.18 ± 0.05
22	Hexyl	Methyl	6.50 ± 0.04[ab]	6.82 ± 0.02[ab]	6.38 ± 0.07[ab]	6.36 ± 0.05[ab]	6.79 ± 0.02[ab]

Inhibition constants expressed as negative logarithms were calculated according to Equation 3. Data are means ± SD from six independent experiments performed in quadruplicate.
*Higher than at other subtypes.
[a]Hexyl higher than butyl.
[b]Methyl higher than hydrogen (multiway ANOVA, Tukey's HSD, $P < 0.01$).

Compound **12** showed slightly higher affinity than compound **11**, compound **22** slightly higher affinity than compound **21** and compound **21** with higher affinity than compound **12** at all receptor subtypes (Table 1; Supporting Information Figure S2).

Inhibitory effects of tested compounds on functional response to carbachol were quantified by measurement of changes in accumulation of inositol phosphates (IP_X). M_2 and M_4 receptors that preferentially inhibit cAMP synthesis *via* $G_{i/o}$ G-proteins were coupled to the PLC *via* promiscuous G_{15} G-protein (Offermanns and Simon, 1995). The response to carbachol was measured at various concentrations of the test compounds. The test compounds concentration-dependently increased the EC_{50} of carbachol and slightly decreased carbachol maximal effect (E_{MAX}) (Supporting Information Figures S3–S6). Changes in E_{MAX} of the functional response implied that the test compounds affected carbachol efficacy, suggesting allosteric or non-competitive interaction. Their inhibition constants (K_B) were obtained by Schild analysis (Figure 2). Inhibition of functional response to carbachol by compound **11** was rather poor with K_B over 10 μM and non-selective (Table 2). In contrast, other compounds tested were more potent at inhibiting the functional response to carbachol and preferentially inhibited M_1 receptors. Except for compound **11**, functional inhibition constants (K_B) were lower than binding inhibition constants (K_i) (Table 2 vs. Table 1), indicative of non-competitive or allosteric inhibition of functional response to carbachol. Accordingly, Equation 5 (describing competitive interaction) fits data only for compound **11** whereas Equation 6 (describing allosteric inhibition) fits best for compounds **12** and **22** at all subtypes. For compound **21**, Equation 5 fits data better than Equation 6 only at M_2 and M_3. In all cases of allosteric interaction between tested compounds and carbachol, negative allosteric inhibition was very strong. However, data from inhibition of 1 nM [^{3}H]-NMS binding by the test compounds did not fit an allosteric interaction (Supporting Information Figure S1).

The nature of the IP_X assay did not allow for binding equilibration of the compounds tested. Therefore, effects of test compounds on carbachol-stimulated [^{35}S]-GTPγS binding after 15 h equilibration were also measured (Supporting Information Figures S3–S6). The test compounds affected [^{35}S]-GTPγS binding in the absence of carbachol (Supporting Information Table S1). In some cases, they increased and in other cases decreased basal [^{35}S]-GTPγS binding. The effects of the compounds tested varied among receptor subtypes. All the compounds tested concentration-dependently increased the EC_{50} of carbachol-stimulated [^{35}S]-GTPγS binding to all subtypes (Supporting Information Table S2). In most cases, increases in EC_{50} were similar at 10 and 100 μM concentration of the compounds tested. The compounds affected the E_{MAX} of carbachol-stimulated [^{35}S]-GTPγS binding (Supporting Information Table S3). In some cases, they increased and in other cases decreased the E_{MAX} of [^{35}S]-GTPγS binding. The effects of the compounds tested varied among receptor subtypes.

Experiments were conducted to detect the binding of the test compounds to the putative secondary binding site dissociation. Rates of [^{3}H]-NMS dissociation were determined at various high concentrations of test compounds. All compounds concentration-dependently slowed down the dissociation of [^{3}H]-NMS. The observed dissociation rate constants (k_{obs}) were then plotted against concentration of test compound used (Figure 3). Equation 8 was fit to data, and apparent equilibrium dissociation constants of test compounds for the receptor-[^{3}H]-NMS complex were calculated (Table 3). A slope of 1 for the curves was obtained in all cases. The resulting K_As varied from 100 μM to 1 mM (from 3.96 ± 0.02 for compound **21** at M_2 to 2.97 ± 0.03 for compound **12** at M_3 receptor, mean ± SD, $n = 3$).

Ability to reverse the inhibitory effects of the text compound on functional responses was tested by washing the compounds out, as described in Methods. While this procedure completely abolished the inhibition of the functional response to carbachol by compounds **11** and **12** (Figure 4), it only partially reduced the inhibition induced by compounds **21** and **22** indicating some resistance to washing (Figure 5, hatched symbols). Extension of washing time for compounds to dissociate from 1 to 5 h further decreased inhibition of functional response to carbachol by compounds **21** and **22** indicating that the washing out of the test compounds was indeed slow (Figure 5, open symbols).

Rates of dissociation of test compounds from receptors were measured in washing experiments as recovery of [^{3}H]-NMS binding to membranes exposed to test compounds (Figure 6). Membranes were first incubated with test compounds at final concentration 100 μM for 1 h. Then

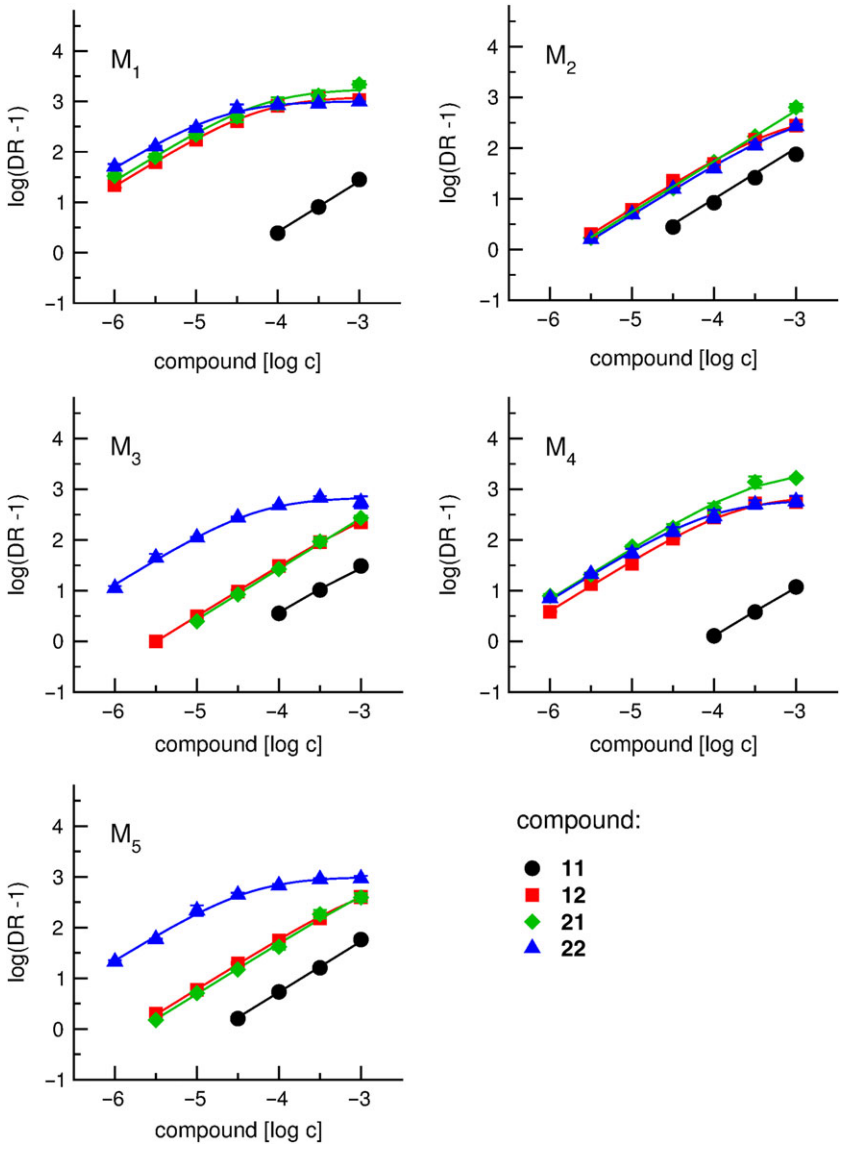

Figure 2

Schild analysis of functional antagonism. The logarithms of dose-response (DR) of half-efficient concentrations (EC_{50}) in the presence of test compound to EC_{50} in the absence of test compound are plotted against concentrations of test compound. Equations 5 or 6 were fitted to data. Resulting inhibition constants (K_B) are summarized in Table 2. Data are means ± SD from three independent experiments performed in triplicate.

Table 2

Inhibition constants of functional response to carbachol

	11		12		21		22	
	pK_B	α	pK_B	α	pK_B	α	pK_B	α
M_1	4.40 ± 0.06	comp	7.41 ± 0.04	0.0010 ± 0.0002	7.48 ± 0.04	0.0010 ± 0.0003	7.68 ± 0.04	0.0011 ± 0.0002
M_2	4.93 ± 0.05	comp	5.81 ± 0.03	0.0014 ± 0.0002	5.73 ± 0.03	comp	5.70 ± 0.03	0.0016 ± 0.0003
M_3	4.53 ± 0.05	comp	5.50 ± 0.02	0.0013 ± 0.0002	5.39 ± 0.04	comp	7.10 ± 0.04	0.0014 ± 0.0003
M_4	4.11 ± 0.06	comp	6.59 ± 0.03	0.0012 ± 0.0002	6.56 ± 0.03	0.0010 ± 0.0002	6.86 ± 0.03	0.0012 ± 0.0002
M_5	4.71 ± 0.05	comp	5.79 ± 0.03	0.0009 ± 0.0002	5.68 ± 0.03	0.0008 ± 0.0003	7.31 ± 0.04	0.0009 ± 0.0002

Inhibition constants K_B and factors of cooperativity were obtained by fitting Equations 5 or 6 to the data from functional response assays in the presence of antagonist. K_Bs are expressed as negative logarithms. Data are means ± SD from three independent experiments performed in triplicate.

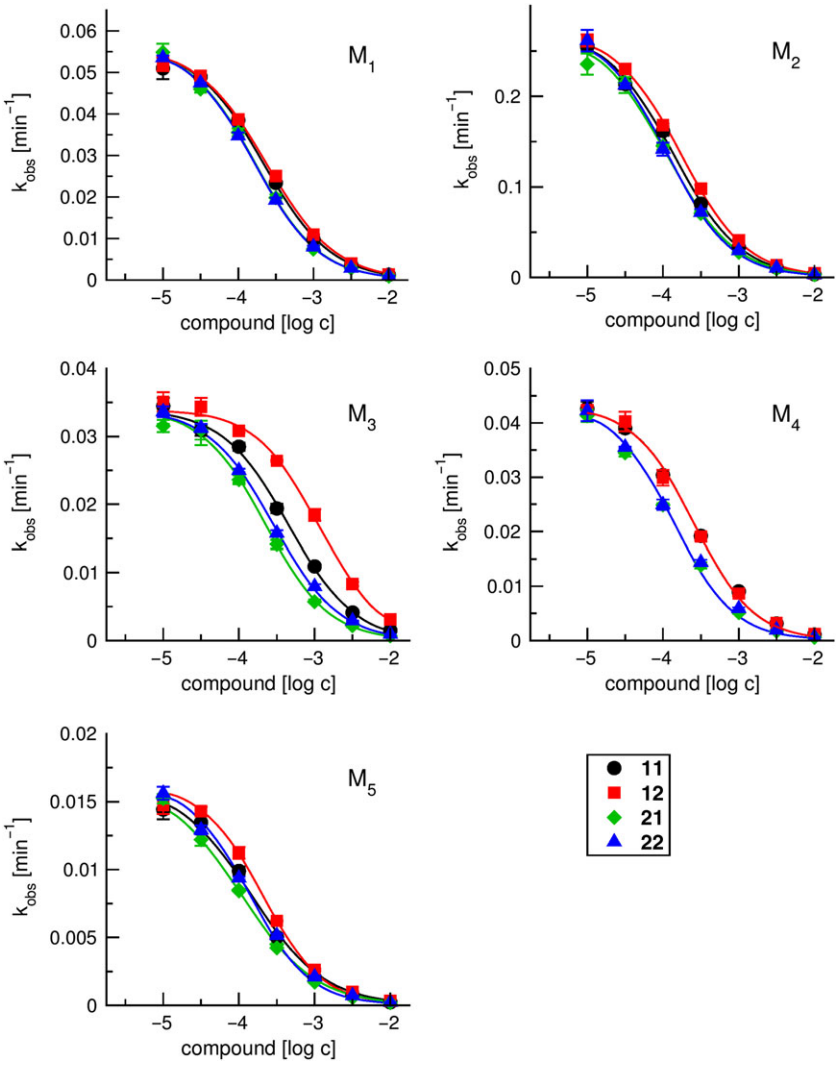

Figure 3

Observed rates of dissociation. Observed dissociation rate of [^{3}H]-NMS from receptors in dissociation experiments is plotted against concentration of compound present during dissociation. Equation 8 was fitted to data to obtain apparent equilibrium dissociation constants (K_A) of compound for receptor-[^{3}H]-NMS complex. The resulting K_As are summarized in Table 3. Data are means ± SD from three independent experiments performed in triplicate.

Table 3

Apparent equilibrium dissociation constants of compounds to receptor-[^{3}H]-NMS complex

	M_1	M_2	M_3	M_4	M_5
11	3.66 ± 0.02	3.86 ± 0.02	3.34 ± 0.03	3.60 ± 0.02	3.84 ± 0.02
12	3.62 ± 0.03	3.77 ± 0.02	2.97 ± 0.03	3.57 ± 0.03	3.70 ± 0.02
21	3.79 ± 0.02	3.96 ± 0.02	3.68 ± 0.02	3.85 ± 0.02	3.95 ± 0.02
22	3.76 ± 0.02	3.91 ± 0.02	3.54 ± 0.02	3.82 ± 0.02	3.85 ± 0.02

Apparent equilibrium dissociation constants K_A of compounds to receptor-[^{3}H]-NMS complex at individual receptor subtypes were calculated according to Equation 8 and are expressed as negative logarithms. Slopes of curves were 1 in all cases. Data are means ± SD from three independent experiments.

membranes were washed 3 times by centrifugation, resuspended in 50-fold excess of incubation medium and incubated for up to 9 h. Membranes were then washed again and incubated for 1 h with 1 nM [^{3}H]-NMS. The data revealed that the dissociation rates of compounds **21** and **22** were much slower than the dissociation rates of compounds

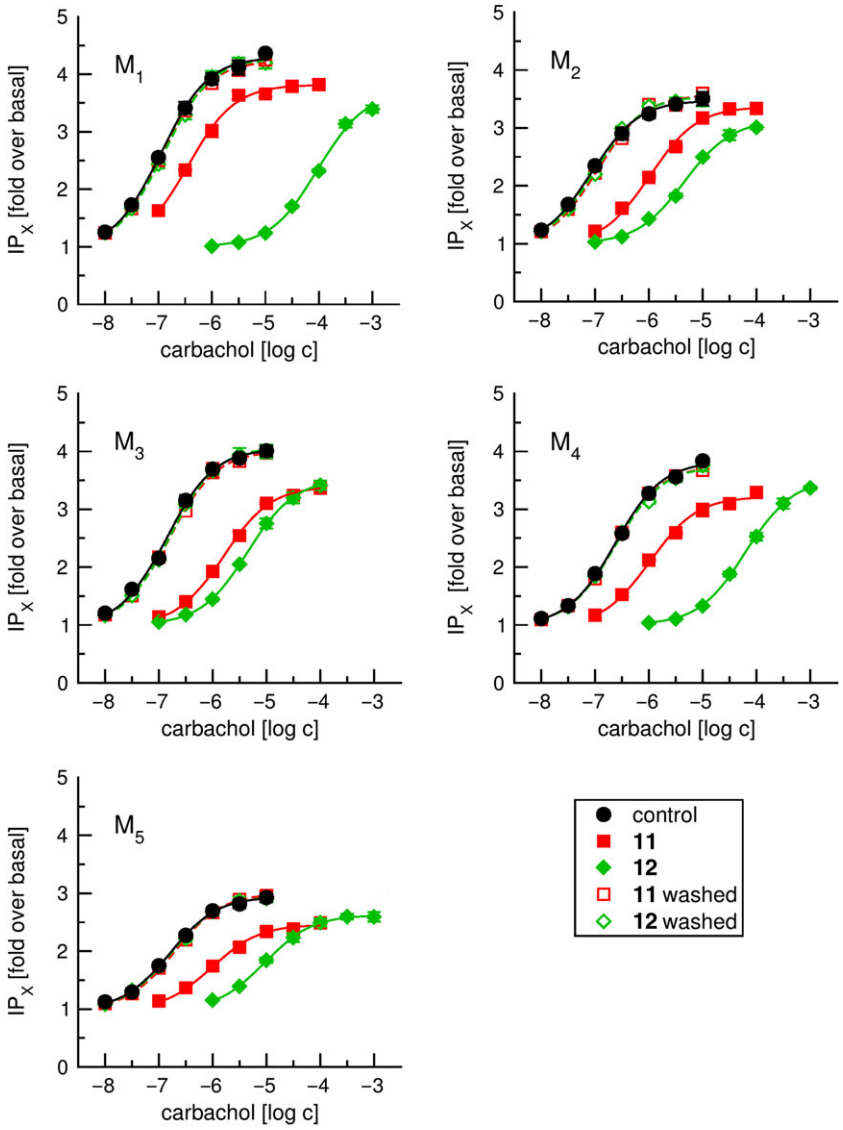

Figure 4

Inhibition of functional response to carbachol by compounds **11** and **12**. Level of inositol phosphates (IP_X) stimulated by carbachol alone (control) or in the presence (solid symbols) of 0.3 mM compound **11** (red) and 0.1 mM compound **12** (green) or after incubation with compounds followed by standard washing (open symbols). Level of IP_X is expressed as fold over basal level and is plotted against concentration of carbachol used to induce a functional response. Data are means ± SD from three independent experiments performed in triplicate.

11 and **12** from all receptor subtypes. Based on recovery of [^{3}H]-NMS binding in washing experiments, half-times of dissociation of the test compounds were estimated (Table 4). As almost all [^{3}H]-NMS binding was recovered after 1 h washing of compounds **11** and **12**, estimates of half-times for these compounds were accompanied by large errors (approximately 25%). In the case of compounds **21** and **22**, for a given subtype, half-times of dissociation were rather similar but differed among receptor subtypes. Dissociation half-times of compound **21** at M_1 and M_4 receptors were about twice as long as half-times at M_2, M_3 and M_5 receptors. Dissociation half-times of compound **22** varied from 4 to 5 h except at M_2 receptors where it was shorter than 2 h.

Discussion

The major finding of this study is that two of the newly synthesized antagonists (Boulos *et al.*, 2018) (Figure 1, compounds **21** and **22**) are long-acting (slowly dissociating) antagonists that preferentially inhibit the M_1 subtype of muscarinic receptors. These compounds and the long-acting agonist xanomeline (Christopoulos *et al.*, 1998) possess a hexyloxy chain that is responsible for the slow dissociation.

Muscarinic receptors mediate a wide range of physiological functions and thus represent possible pharmacological targets. Specifically, selective M_2 and/or M_3 muscarinic antagonists may be good drug candidates for the treatment of smooth muscle-related disorders, such as airway-associated

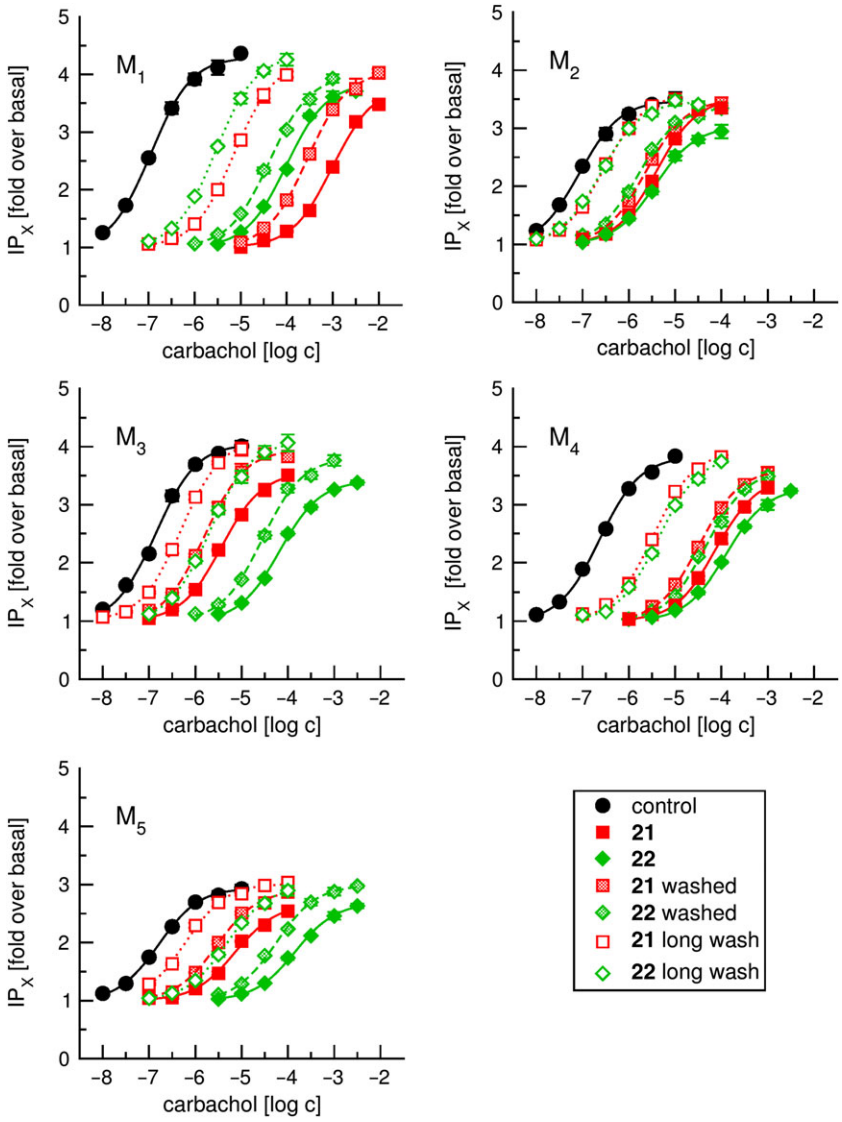

Figure 5

Inhibition of functional response to carbachol by compounds **21** and **22**. Level of inositol phosphates (IP_X) stimulated by carbachol alone (control) or in the presence (solid symbols) of 0.1 mM compound **21** (red) and **22** (green) or after incubation with compounds followed by standard (hatched symbols) or extended (open symbols) washing. Level of IP_X is expressed as fold over basal level and is plotted against concentration of carbachol used to induce a functional response. Data are means ± SD from three independent experiments performed in triplicate.

disorders like asthma and over-reactive bladder syndrome (Ehlert, 2003). M_1 or M_4 selective muscarinic antagonists are associated with possible treatments for PD (Jeon *et al.,* 2010; Lester *et al.,* 2010; Xiang *et al.,* 2012). M_5 antagonists may provide a novel therapeutic approach for drug addiction (Thomsen *et al.,* 2005; Eglen, 2012). In view of these findings, it is quite possible that subtype-selective muscarinic antagonists may be useful therapeutic drugs for several disease states with reduced side effects.

Crystallographic studies of the cloned muscarinic receptors have revealed that structures of individual subtypes are virtually identical, particularly at transmembrane helices II–VII, a region containing highly conserved hydrophilic side groups that form the vestibule for the orthosteric binding site, the orthosteric binding site itself and receptor activation network (Haga *et al.,* 2012; Kruse *et al.,* 2012; Thal *et al.,* 2016). Given that the orthosteric site is highly conserved among subtypes of muscarinic receptors, orthosteric ligands must overcome many limitations such as low binding selectivity. Functionally selective agonists with similar affinity for all subtypes of muscarinic receptors but preferentially activate the M_1 receptor have been discovered (Shannon *et al.,* 1994; Langmead *et al.,* 2006). From these findings, it is conceivable for antagonists to preferentially inhibit a particular receptor subtype while staying non-selective in binding. Besides the high potency, long-residence time is a desired feature of antagonists. Antagonists with long-residence time tend to inhibit the receptor for a longer duration, thus lower doses to reach a therapeutic effect are required. It has been shown that wash-resistance of the long-acting muscarinic

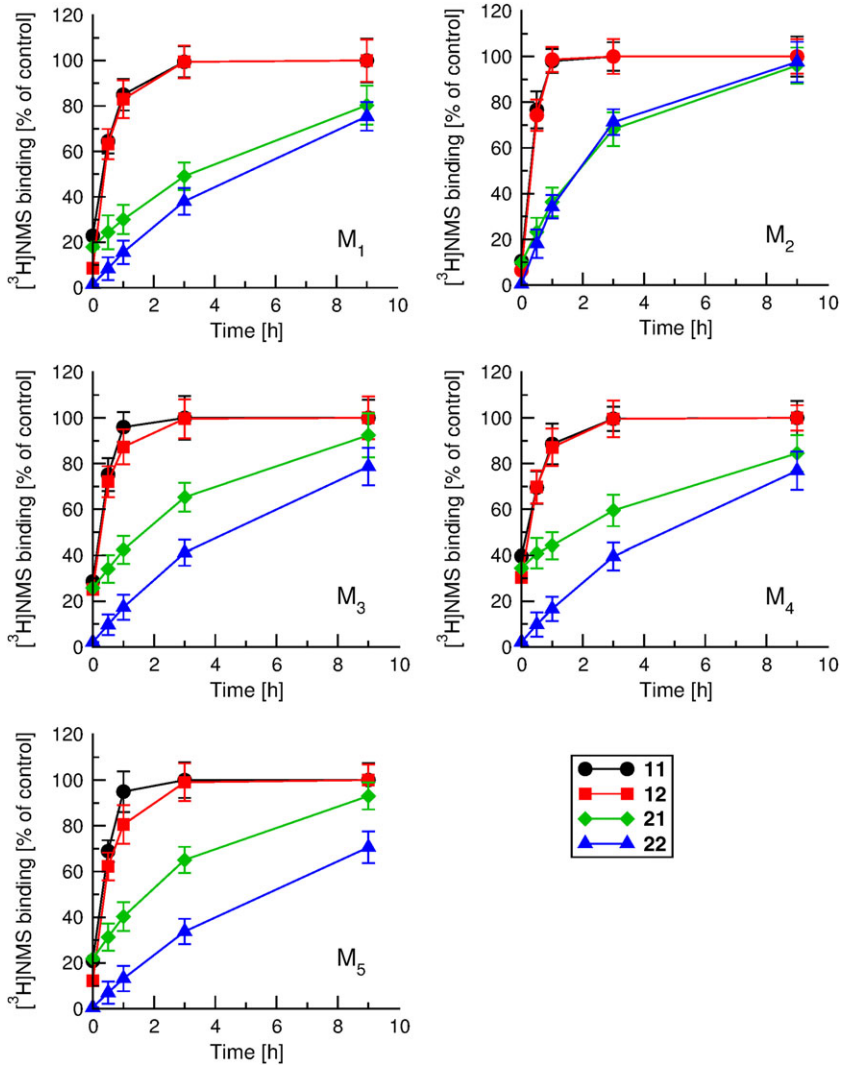

Figure 6

Dissociation kinetics of compounds from muscarinic receptors. Membranes were incubated with test compounds at 100 μM concentration then washed by centrifugation and allowed to dissociate in a 50-fold excess of incubation medium for the time indicated on abscissa and washed again. Samples were then incubated with [^{3}H]-NMS for 1 h. [^{3}H]-NMS binding is expressed as percentage of binding to membranes not exposed to compounds. Data are means ± SD of three experiments performed in triplicate.

Table 4

Estimates of dissociation half-times

	11	12	21	22
M_1	0.4 ± 0.1	0.4 ± 0.1	4.4 ± 0.4[a]	4.5 ± 0.4[a]
M_2	0.2 ± 0.1	0.2 ± 0.1	2.0 ± 0.2[b]	1.7 ± 0.2[b]
M_3	0.2 ± 0.1	0.4 ± 0.1	2.7 ± 0.3[b]	4.1 ± 0.3[a]
M_4	0.4 ± 0.1	0.4 ± 0.1	4.3 ± 0.4[a]	4.3 ± 0.4[a]
M_5	0.3 ± 0.1	0.5 ± 0.1	2.6 ± 0.3[b]	5.1 ± 0.4[a]

Dissociation half-times expressed in h were estimated based on the recovery of [^{3}H]-NMS binding in washing experiments (Figure 6). Data are means ± SD from six independent experiments performed in triplicate. Comp, competitive inhibition. Values in [a] are higher than those in [b] ($P < 0.01$, ANOVA, Tukey's HSD post test).

agonist xanomeline is due to the presence of a hexyloxy chain in its structure (Jakubík *et al.*, 2004).

In general, muscarinic antagonists are bulkier and contain an aromatic ring next to the electronegative region. The distance between the electronegative and electropositive regions is also greater compared with agonists. These features were taken into consideration during the design and synthesis of N-substituted tetrahydropyridinium-based muscarinic antagonists (Figure 1, compounds **11**, **12**, **21** and **22**), structurally related to the agonist xanomeline, in order to validate this concept. Moreover, since xanomeline has been found to have higher affinity and potency than its analogues with shorter alkoxy chains, compounds **21** and **22** with hexyloxy chains were also expected to show similar pharmacological profiles. In addition, butyloxy derivatives **11** and **12** were also synthesized for comparison.

Compared with the xanomeline affinity of about 100 nM at all subtypes of muscarinic receptors (Jakubík *et al.,* 2008), the affinity of the test compounds is in micromolar range at all receptor subtypes (Table 1), except for compound **22** with affinity around 300 nM. The high affinity observed for xanomeline is the result of extensive structure optimization. Since the test compounds are bulkier than xanomeline, they probably do not fit the binding site as well resulting in their lower affinity. Xanomeline also has a higher affinity than its analogues with shorter O-alkyl chains (Jakubík *et al.,* 2004). Correspondingly, compound **22** (R_1 = hexyl) also has a higher affinity than compound **12** (R_1 = butyl). Thus, similar to xanomeline, the hexyloxy chain also contributes to the higher affinity of antagonists tested. In general, muscarinic ligands with a quaternary nitrogen have higher affinity than ligands with a tertiary nitrogen. Accordingly, compounds **12** and **22** (R_2 = methyl) have higher affinity than compounds **11** and **21** (R_2 = hydrogen).

All the compounds tested inhibited the functional response to carbachol in sub-micromolar range, except for compound **11** (Figure 2, Table 2). Although xanomeline has the same binding affinity at all subtypes of muscarinic receptors (Jakubík *et al.,* 2008), it preferentially activates M_1 receptors (Bymaster *et al.,* 1998; Woolley *et al.,* 2009; Šantrůčková *et al.,* 2014; Bradley *et al.,* 2017). Similarly, except for compound **11**, the test compounds preferentially inhibit M_1 receptors despite having the same binding affinity at all receptor subtypes. Schild analysis of functional antagonism suggests an allosteric mode of interaction for all compounds, except for **11** (Table 2). The potency of the test compounds to inhibit the functional response to carbachol (pK_B) is greater than binding affinity (pK_i), except compound **11**, indicating non-competitive or allosteric inhibition of functional response to carbachol (Table 2 vs. 1). Under equilibrium, the competitive antagonism equilibrium dissociation constant of an antagonist K_B, determined in functional assays, should be equal to the equilibrium dissociation constant K_i, determined in binding assays. The slow dissociation of the test compounds (Figure 6) and their micromolar affinity indicate slow association. This in turn indicates that the binding of the test compounds is not under equilibrium in these functional assays. On the other hand, the binding of carbachol is very fast and reaches equilibrium under these experimental conditions. These hemi-equilibrium conditions mean that the test compounds inhibit the response to carbachol to a lesser extent than they would have under equilibrium, resulting in an underestimation of antagonist pK_B (e.g. compound **22** at M_2 receptor). However, the pK_B of the test compounds is actually greater than the pK_i in most of cases. Hemi-equilibrium conditions should have resulted in Schild plots with slopes lower than 1, contrary to Schild plots with slopes of 1 for all the antagonists tested at all receptors. These results indicate a secondary binding site to which test compounds bind to under equilibrium, in functional assays, with an affinity corresponding to the K_B (i.e. higher than affinity for the orthosteric binding site with affinity corresponding to the K_i). Similar fast association, slow dissociation and apparent affinity that does not correspond to binding kinetics have been observed for xanomeline (Jakubik *et al.,* 2002). The binding to the secondary site is not observed in binding experiments, probably due to lack of interference with [^{3}H]-NMS binding. Another indicator of allosteric (e.g. antagonists that allosterically decrease affinity and or efficacy of carbachol) or non-competitive (e.g. antagonists that do not affect agonist binding but prevent receptor activation) interaction of tested compounds are changes in E_{MAX} of functional response to carbachol. The saturation of antagonism of tested compounds at high concentrations suggests allosteric rather than non-competitive interaction (Supporting Information, Figures S3–S6).

To measure functional antagonism of test compounds under equilibrium binding to the orthosteric site, [^{35}S]-GTPγS binding was measured after 15 h preincubation of membranes with carbachol and test compounds (Supporting Information Figures S7–S10). The test compounds changed [^{35}S]-GTPγS binding in the absence of carbachol (Supporting Information Table S1). The observed decrease in basal [^{35}S]-GTPγS binding may be explained as inverse agonism of test compounds at muscarinic receptors. However, the observed increase in basal [^{35}S]-GTPγS binding indicates that the test compounds act either directly at G-proteins or at endogenous (other than muscarinic) GPCRs. All the compounds tested concentration-dependently increased EC_{50} of carbachol-stimulated [^{35}S]-GTPγS binding at all receptor subtypes (Supporting Information Table S2). Pleiotropy of effects of test compounds on [^{35}S]-GTPγS binding makes rigorous analysis of carbachol-stimulated [^{35}S]-GTPγS binding impossible. In most cases, similar EC_{50} values of carbachol-stimulated [^{35}S]-GTPγS binding at both 10 and 100 μM concentration indicate negative allosteric modulation of carbachol-stimulated [^{35}S]-GTPγS binding by the test compound. Changes in E_{MAX} of carbachol-stimulated [^{35}S]-GTPγS binding further support the allosteric mode of action of the test compounds (Supporting Information Table S3).

The secondary binding site for the orthosteric antagonists NMS and quinuclidinyl benzilate, which is located between the second and the third extracellular loops of muscarinic receptors was previously identified using dissociation experiments (Jakubík *et al.,* 2017). All test compounds also slowed down the dissociation of [^{3}H]-NMS in this experimental setup (Figure 3). Calculated affinities of the receptor-[^{3}H]-NMS complex for test compounds are very low and vary from 100 μM to 1 mM (Table 3). However, in a likely case of negative cooperativity between the binding of [^{3}H]-NMS and test compound, the affinity of a compound for an empty receptor may be much higher than for the receptor-[^{3}H]-NMS complex (Jakubík *et al.,* 2000). Unfortunately, the affinity of the test compounds for the secondary binding site cannot be determined due to competition with [^{3}H]-NMS for the orthosteric binding site.

Unlike compounds **11** and **12** (R_1 = butyl), compounds **21** and **22** (R_1 = hexyl) antagonized the functional response to carbachol even after extensive, 5 h long, washing (Figures 4 and 5). Similar to the long-acting agonist xanomeline, the hexyloxy chain is responsible for resistance to washing (Jakubík *et al.,* 2004). The kinetics of compound dissociation from receptors was measured as a recovery of [^{3}H]-NMS binding to the membranes exposed to compounds followed by washing (Figure 6). Dissociation of compounds **21** and **22**

was slower than dissociation of compounds **11** and **12** (Table 4). However, dissociation half-times of compounds **21** and **22** were about 6 times shorter than the dissociation half-time of xanomeline from M_1 receptors (Jakubík *et al.*, 2004). Thus, some other structural features contribute to the extremely slow dissociation of xanomeline from muscarinic receptors. There are two major differences between xanomeline and compound **21**. Firstly, the distance between the O-hexyl chain and electronegative region in compound **21** is greater than in xanomeline. Secondly, the electronegative region of compound **21** is more negative than that of xanomeline. These differences may result in a weaker interaction of the O-hexyl chain of compound **21** with the receptor and consequently to shorter residence time. Moreover, xanomeline is an agonist whereas compound **21** is an antagonist. It is possible that the O-hexyl chain of xanomeline interacts better with a receptor in an active conformation leading to a longer residence-time.

In summary, 1-{2-[4-(hexyloxy)benzoyloxy]ethyl}-1,2,3,6-tetrahydropyridin-1-ium (compound **21**) and 1-{2-[4-(hexyloxy)benzoyloxy]ethyl}-1-methyl-3,6-dihydro-2H-pyridin-1-ium (compound **22**) are potent long-acting M_1-preferring antagonists. These and other structurally related M_1-selective antagonists may have therapeutic potential for striatal cholinergic dystonia, delaying epileptic seizure after organophosphate intoxication or relieving depression. These compounds may also serve as a tool in research into cognitive deficits.

Acknowledgements

This work was supported by the Czech Academy of Sciences support [RVO:67985823], the Grant Agency of the Czech Republic grant [17-16182S] and the Physical Science Department at Barry University.

Author contributions

J.J., J.B. and V.D. participated in research design; A.R., V.R. and J.J. conducted experiments; J.B. contributed new compounds; A.R. and J.J. performed data analysis; J.J., A.R., V.D. and J.B. wrote or contributed to the writing of the manuscript; all authors read and approved the final version of manuscript.

Conflict of interest

The authors declare no conflicts of interest.

Declaration of transparency and scientific rigour

This Declaration acknowledges that this paper adheres to the principles for transparent reporting and scientific rigour of preclinical research recommended by funding agencies, publishers and other organisations engaged with supporting research.

References

Alexander SPH, Christopoulos A, Davenport AP, Kelly E, Marrion NV, Peters JA *et al.* (2017). The Concise Guide to PHARMACOLOGY 2017/18: G protein-coupled receptors. Br J Pharmacol 174: S17–S129.

Bonner TI (1989). The molecular basis of muscarinic receptor diversity. Trends Neurosci 12: 148–151.

Boulos JF, Jakubik J, Boulos JM, Randakova A, Momirov J (2018). Synthesis of novel and functionally selective non-competitive muscarinic antagonists as chemical probes. Chem Biol Drug Des 91: 93–104.

Bradley SJ, Bourgognon JM, Sanger HE, Verity N, Mogg AJ, White DJ *et al.* (2017). M1 muscarinic allosteric modulators slow prion neurodegeneration and restore memory loss. J Clin Invest 127: 487–499.

Bymaster FP, Carter PA, Peters SC, Zhang W, Ward JS, Mitch CH *et al.* (1998). Xanomeline compared to other muscarinic agents on stimulation of phosphoinositide hydrolysis *in vivo* and other cholinomimetic effects. Brain Res 795: 179–190.

Cheng Y, Prusoff WH (1973). Relationship between the inhibition constant (K1) and the concentration of inhibitor which causes 50 per cent inhibition (I50) of an enzymatic reaction. Biochem Pharmacol 22: 3099–3108.

Christopoulos A, Pierce TL, Sorman JL, El-Fakahany EE (1998). On the unique binding and activating properties of xanomeline at the M1 muscarinic acetylcholine receptor. Mol Pharmacol 53: 1120–1130.

Curtis MJ, Bond RA, Spina D, Ahluwalia A, Alexander SP, Giembycz MA *et al.* (2015). Experimental design and analysis and their reporting: new guidance for publication in BJP. Br J Pharmacol 172: 3461–3471.

Disse B, Reichl R, Speck G, Traunecker W, Rominger KL, Hammer R (1993). Ba 679 BR, A novel long-acting anticholinergic bronchodilator. Life Sci 52: 537–544.

Eglen RM (2012). Overview of muscarinic receptor subtypes. In: Fryer AD, Christopoulos A, Nathanson NM (eds). Muscarinic Receptors, Springer-Verlang Berlin Heidelberg Handb Exp Pharmacol, Vol. 208, pp. 3–28.

Ehlert FJ (2003). Contractile role of M2 and M3 muscarinic receptors in gastrointestinal, airway and urinary bladder smooth muscle. Life Sci 74: 355–366.

El-Fakahany EE, Jakubík J (2016). Radioligand binding at muscarinic receptors. In: Myslivecek J, Jakubik J (eds). Muscarinic Receptor: From Structure to Animal Models, Humana Press, New York. Neuromethods 107: 37–68.

Eskow Jaunarajs KL, Bonsi P, Chesselet MF, Standaert DG, Pisani A (2015). Striatal cholinergic dysfunction as a unifying theme in the pathophysiology of dystonia. Prog Neurobiol 127–128: 91–107.

Haga K, Kruse AC, Asada H, Yurugi-Kobayashi T, Shiroishi M, Zhang C *et al.* (2012). Structure of the human M2 muscarinic acetylcholine receptor bound to an antagonist. Nature 482: 547–551.

Harding SD, Sharman JL, Faccenda E, Southan C, Pawson AJ, Ireland S *et al.* (2018). The IUPHAR/BPS Guide to PHARMACOLOGY in 2018: updates and expansion to encompass the new guide to IMMUNOPHARMACOLOGY. Nucl Acids Res 46: D1091–D1106.

Heusler P, Cussac D, Naline E, Tardif S, Clerc T, Devillier P (2015). Characterization of V0162, a new long-acting antagonist at human M3 muscarinic acetylcholine receptors. Pharmacol Res 100: 117–126.

Jakubík J, El-Fakahany EE, Tuček S (2000). Evidence for a tandem two-site model of ligand binding to muscarinic acetylcholine receptors. J Biol Chem 275: 18836–18844.

Jakubík J, Michal P, Machová E, Doležal V (2008). Importance and prospects for design of selective muscarinic agonists. Physiol Res 57: S39–S47.

Jakubík J, Randáková A, Zimčík P, El-Fakahany EE, Doležal V (2017). Binding of N-methylscopolamine to the extracellular domain of muscarinic acetylcholine receptors. Sci Rep 7: 40381.

Jakubík J, Tuček S, El-Fakahany EE (2002). Allosteric modulation by persistent binding of xanomeline of the interaction of competitive ligands with the M1 muscarinic acetylcholine receptor. J Pharmacol Exp Ther 301: 1033–1041.

Jakubík J, Tuček S, El-Fakahany EE (2004). Role of receptor protein and membrane lipids in xanomeline wash-resistant binding to muscarinic M1 receptors. J Pharmacol Exp Ther 308: 105–110.

Jeon J, Dencker D, Wortwein G, Woldbye DPD, Cui Y, Davis AA *et al*. (2010). A subpopulation of neuronal M4 muscarinic acetylcholine receptors plays a critical role in modulating dopamine-dependent behaviors. J Neurosci 30: 2396–2405.

Kenakin TP (2014). Allosteric modulation. In: Kenakin TP (ed). A Pharmacology Primer: Techniques for More Effective and Strategic Drug Discovery. Academic Press: New York, NY, pp. 155–179.

Klinkenberg I, Blokland A (2010). The validity of scopolamine as a pharmacological model for cognitive impairment: A review of animal behavioral studies. Neurosci Biobehav Rev 34: 1307–1350.

Kruse AC, Hu J, Pan AC, Arlow DH, Rosenbaum DM, Rosemond E *et al*. (2012). Structure and dynamics of the M3 muscarinic acetylcholine receptor. Nature 482: 552–556.

Langmead CJ, Fry VAH, Forbes IT, Branch CL, Christopoulos A, Wood MD *et al*. (2006). Probing the molecular mechanism of interaction between 4-n - and the muscarinic M 1 receptor: direct pharmacological evidence that AC-42 is an allosteric agonist. Mol Pharmacol 69: 236–246.

Lazareno S, Birdsall NJ (1995). Detection, quantitation, and verification of allosteric interactions of agents with labeled and unlabeled ligands at G protein-coupled receptors: interactions of strychnine and acetylcholine at muscarinic receptors. Mol Pharmacol 48: 362–378.

Lester DB, Rogers TD, Blaha CD (2010). Acetylcholine-dopamine interactions in the pathophysiology and treatment of CNS disorders. CNS Neurosci Ther 16: 137–162.

Miller SL, Aroniadou-Anderjaska V, Pidoplichko VI, Figueiredo TH, Apland JP, Krishnan JKS *et al*. (2017). The M1 muscarinic receptor antagonist VU0255035 delays the development of status epilepticus after organophosphate exposure and prevents hyperexcitability in the basolateral amygdala. J Pharmacol Exp Ther 360: 23–32.

Navarria A, Wohleb ES, Voleti B, Ota KT, Dutheil S, Lepack AE *et al*. (2015). Rapid antidepressant actions of scopolamine: role of medial prefrontal cortex and M1-subtype muscarinic acetylcholine receptors. Neurobiol Dis 82: 254–261.

Offermanns S, Simon MI (1995). G alpha 15 and G alpha 16 couple a wide variety of receptors to phospholipase C. J Biol Chem 270: 15175–15180.

Prat M, Fernández D, Buil MA, Crespo MI, Casals G, Ferrer M *et al*. (2009). Discovery of novel quaternary ammonium derivatives of (3R)-quinuclidinol esters as potent and long-acting muscarinic antagonists with potential for minimal systemic exposure after inhaled administration: identification of (3 R)-3-{[Hydroxy(di-2-thienyl)a. J Med Chem 52: 5076–5092.

Šantrůčková E, Doležal V, El-Fakahany EE, Jakubík J (2014). Long-term activation upon brief exposure to xanomleline is unique to M1 and M4 subtypes of muscarinic acetylcholine receptors. PLoS One 9: e88910.

Shannon HE, Bymaster FP, Calligaro DO, Greenwood B, Mitch CH, Sawyer BD *et al*. (1994). Xanomeline: a novel muscarinic receptor agonist with functional selectivity for M1 receptors. J Pharmacol Exp Ther 269: 271–281.

Thal DM, Sun B, Feng D, Nawaratne V, Leach K, Felder CC *et al*. (2016). Crystal structures of the M1 and M4 muscarinic acetylcholine receptors. Nature 531: 335–340.

Thomsen M, Woldbye DPD, Wo G, Fink-jensen A, Caine SB (2005). Reduced cocaine self-administration in muscarinic M5 acetylcholine receptor-deficient mice. J Neurosci 25: 8141–8149.

Ulrik CS (2012). Once-daily glycopyrronium bromide, a long-acting muscarinic antagonist, for chronic obstructive pulmonary disease: a systematic review of clinical benefit. Int J Chron Obstruct Pulmon Dis 7: 673–678.

Woolley ML, Carter HJ, Gartlon JE, Watson JM, Dawson LA (2009). Attenuation of amphetamine-induced activity by the non-selective muscarinic receptor agonist, xanomeline, is absent in muscarinic M4 receptor knockout mice and attenuated in muscarinic M1 receptor knockout mice. Eur J Pharmacol 603: 147–149.

Xiang Z, Thompson AD, Jones CK, Lindsley CW, Conn PJ (2012). Roles of the M1 muscarinic acetylcholine receptor subtype in the regulation of basal ganglia function and implications for the treatment of Parkinson's disease. J Pharmacol Exp Ther 340: 595–603.

Supporting Information

Additional Supporting Information may be found online in the supporting information tab for this article.

https://doi.org/10.1111/bph.14187

Figure S1 Competition with [^{3}H]NMS binding.
Figure S2 ANOVA of inhibition constants.
Figure S3 Compound 11 antagonism of functional response to carbachol.
Figure S4 Compound 12 antagonism of functional response to carbachol.
Figure S5 Compound 21 antagonism of functional response to carbachol.
Figure S6 Compound 22 antagonism of functional response to carbachol.
Figure S7 Compound 11 antagonism of carbachol stimulated [^{35}S]GTPγS binding.
Figure S8 Compound 12 antagonism of carbachol stimulated [^{35}S]GTPγS binding.
Figure S9 Compound 21 antagonism of carbachol stimulated [^{35}S]GTPγS binding.
Figure S10 Compound 22 antagonism of carbachol stimulated [^{35}S]GTPγS binding.
Table S1 Effect of tested compounds on basal [^{35}S]GTPγS binding.
Table S2 Effect of tested compounds on EC50 of [^{35}S]GTPγS binding.
Table S3 Effect of tested compounds on ECMAX of [^{35}S]GTPγS binding.